A surge and choke capable compressor flow model: Validation and extrapolation capability

Oskar Leufvén and Lars Eriksson

Original Publication:

Oskar Leufvén and Lars Eriksson, A surge and choke capable compressor flow model: Validation and extrapolation capability, 2013, Control Engineering Practice, (21), 12, 1871-1883.
http://dx.doi.org/10.1016/j.conengprac.2013.07.005

Control Engineering Practice 21 (2013) 1871–1883

Contents lists available at ScienceDirect

Control Engineering Practice

journal homepage: www.elsevier.com/locate/conengprac

A surge and choke capable compressor flow model—Validation and extrapolation capability

Oskar Leufvén *, Lars Eriksson

Division of Vehicular Systems, Department of Electrical Engineering, Linköping University, SE-58183 Linköping, Sweden

ARTICLE INFO

Article history:
Received 30 April 2012
Accepted 10 July 2013
Available online 7 September 2013

Keywords:
Automotive
Restriction
Survey
Surge cycle

ABSTRACT

Increasingly stringent emissions legislation combined with consumer performance demand has created the need for complex automotive engines. The control of this complex system relies heavily on control oriented models. Models capable of describing all operating modes of the systems are beneficial, and the models should be easily parametrized and enable extrapolation. A large database of automotive compressor maps is characterized, and used to develop, validate and automatically parametrize a compressor flow model capable of describing reversed flow, normal operation and choke. Measurement data from both an engine test stand and a surge test stand is used to parametrize and validate the surge capability of the model. The model is shown to describe all modes of operation with good performance, and also to be able to extrapolate to small turbo speeds. The extrapolation capability is important, since compressor maps are shown to lack information for low speeds, even though they frequently operate there in an engine installation.

1. Introduction

Efficiency demands and emissions legislation have lead both heavy duty and car manufacturers to develop ever more advanced turbocharged engines (Emmenthal, Hagemann, & Hucho, 1979; Guzzella, Wenger, & Martin, 2000; Petitjean, Bernardini, Middlemass, Shahed, & Hurley, 2004). The complexity of the charging systems is increasing. Currently e.g. series sequential (Chasse et al., 2008; Galindo, Climent, Guardiola, & Domenech, 2009; Zhang, Deng, Wang, & Zhu, 2008), parallel sequential (Borila, 1988; Thomasson & Eriksson, 2011) systems or a combination of a turbo and a mechanical compressor is in production. Both more stages (Nitta, Minato, & Shimazaki, 2011) as well as the inclusion of electric machines connected to a turbo or a mechanical compressor shaft are being investigated (Eriksson, Lindell, Leufvén, & Thomasson, 2012).

The engine control system plays an important role in achieving the desired turbocharged system behavior. The control system, in turn, relies on good control oriented models for numerous applications e.g. observer design (Höckerdal, Frisk, & Eriksson, 2011), control (García-Nieto, Martínez, Blasco, & Sanchis, 2008; Moulin & Chauvin, 2011; Omran, Younes, & Champoussin, 2009; Shehata, Abdullah, & Areed, 2009), and diagnosis (Kimmich, Schwarte, & Isermann, 2005; Nyberg & Stutte, 2004). The aim of this paper is to collect the state of the art in compressor knowledge and develops a control oriented compressor model, that is directly useful in control, estimation and diagnosis applications.

In automotive applications, a turbocharged (TC) engine operates its turbo, or turbos, with turbo speeds from stand still up to roughly half of the capacity in the manufacturer map. At higher altitudes, a higher pressure ratio (Π_c) is needed, which means that also higher speeds can be reached, see e.g. Olsson (2007). The range of maximum engine torque of a TC engine is related to the flow range of the compressors used, where surge limits the torque at low engine speeds, and choke and over-speeding limit the torque at high engine speeds (see e.g. Leufvén & Eriksson, 2012). Further, a single stage system can be operated with Π_c below unity, e.g. during engine transients before it has overcome inertia effects (Casey & Schlegel, 2010). The, for multi-stage systems, commonly used passive high pressure stage (HP) by-pass (BP) valve (a spring pre-loaded valve that opens for a large enough pressure drop across it) will, in fact, force the HP stage compressor to operate at $\Pi_c < 1$ when charging with the low pressure (LP) stage. This operation also exists as a fail-safe mode for an actively controlled BP valve, see e.g. Fig. 4(a) where the HP stage is operated stationary with $\Pi_c < 1$.

Turbo performance is commonly measured by the turbo manufacturer and represented using maps, see Fig. 1 for a sketch. Normally the map focuses on regions of high engine performance, i.e. torque and power, while the majority of engine operation is spent in regions that are not covered in the standard maps. Neither surge nor choke operation is covered in a standard map.

* Corresponding author. Tel.: +46 13 281994; fax: +46 13 139282.
E-mail addresses: oleufven@isy.liu.se (O. Leufvén), larer@isy.liu.se (L. Eriksson).

0967-0661/$ - see front matter © 2013 Elsevier Ltd. All rights reserved.
http://dx.doi.org/10.1016/j.conengprac.2013.07.005

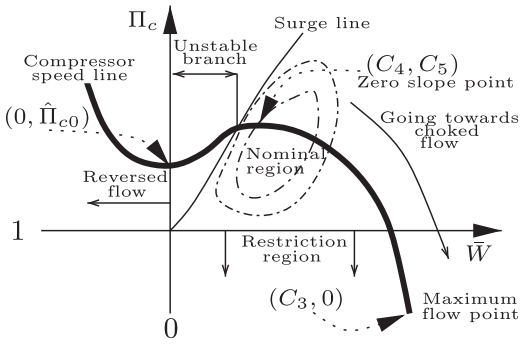

Fig. 1. All three turbo compressor operation quadrants important to model for automotive control applications. One speed line with constant $\overline{N}$ is shown. The islands show contours of constant adiabatic efficiency. Some important speed line points are also marked: pressure ratio at zero flow point $(0, \hat{\Pi}_{c0})$, corrected mass flow and pressure ratio at the zero slope line (ZSL) point with positive flow $(\overline{W}_{\mathrm{ZSL}}, \hat{\Pi}_{\mathrm{ZSL}})$, and the maximum flow point at zero pressure ratio $(\overline{W}_{max}, 0)$. These will be used in the Ellipse flow model structure presented in Section 5.2. Note also that the surge line does not necessarily pass through the ZSL point of a speed line.

A control oriented model should thus preferably be able to describe all modes of operation has good extrapolation capability, and be easy to tune with the restricted available map data.

1.1. Contributions and outline

This paper analyzes and extends the control oriented Ellipse compressor model that was proposed for car applications in Leufvén and Eriksson (2011). The model is capable of capturing all modes of operation (normal, surge and choke/restriction), and avoids heat transfer modeling through its emphasis on mass flow to pressure ratio characteristics.

This paper contributes with an analysis of map properties for a database with 236 maps, for applications ranging from small automotive to large heavy duty. The data distribution is discussed, and what a practicing engineer can encounter when working with modeling and parameter estimation of compressor data is highlighted. The knowledge generated in the analysis of the compressor maps is later used for the parametrization process of the proposed model structure. A compressor flow modeling literature survey covering all operating modes is then presented. An in-depth analysis of the Ellipse model structure follows. The analysis presents a novel automated parametrization process used on the database maps. The Ellipse model structure is extended and further validated to also include heavy duty application maps. The model structure is validated on the database of compressor maps, and an analysis focusing on the model structure extrapolation capability is presented. Summary and conclusions end the paper.

2. The compressor map

The goal of the map is to describe the compressor performance, for all operating conditions. When turbocharger performance is measured, the characteristics obtained are valid for the inlet conditions under which the measurements were conducted. To overcome this deficiency, different correction factors are applied to scale the performance variables to cover other inlet conditions. The correction factors are based on the dimensional analysis of the compression system (Dixon & Hall, 2010). Most maps use corrected mass flow

$$\overline{W} = W_c \frac{\sqrt{T_{01}/T_{std}}}{p_{01}/p_{std}} \tag{1}$$

and corrected shaft speed

$$\overline{N} = \frac{N_{tc}}{\sqrt{T_{01}/T_{std}}} \tag{2}$$

where p_{std} and T_{std} are referred to as reference conditions, T_{01} and p_{01} are the temperature and the pressure at the compressor inlet respectively, and W_c and N_{tc} are the compressor mass flow and the shaft speed respectively (the nomenclature is provided in Appendix A). The reference conditions are a key component, and must be provided in the map. The bar denotes a corrected quantity, and the compressor model of this paper is given in corrected quantities. An experimental investigation of compressor correction quantities for automotive applications is presented in Leufvén and Eriksson (2012), demonstrating the importance and correctness of Eqs. (1) and (2).

The compressor map, see e.g. Fig. 1, shows stationary pressure ratio, $\Pi_c = p_{02}/p_{01}$, and adiabatic efficiency, η_c, a compressor achieves as a function of $\overline{W}$ and $\overline{N}$. Here p_{02} is the pressure in the control volume after the compressor. When the compressor is installed as a part of an engine, these pressures are commonly referred to the air filter control volume pressure $p_{af}(=p_{01})$ and compressor control volume pressure $p_c(=p_{02})$. Points of equal $\overline{N}$ are normally connected, giving a compressor speed line, denoted SpL. Points are measured from the smallest mass flow, found at the surge line, to the largest mass flow where choking can occur. Choke can lead to a pressure drop over the compressor. Surge is a dangerous instability and can occur e.g. during a gear shift under acceleration, where a throttle closing causes a fast reduction in mass flow.

2.1. Map measurement

The common way to measure a turbo map is in a gas stand (Heywood, 1988; Watson & Janota, 1982; Zinner, 1985). However, also other facilities can be used, see e.g. Galindo, Serrano, Guardiola, and Cervelló (2006) and Leufvén and Eriksson (2010). Methods for both single stage and multiple stage systems are presented (Westin & Burenius, 2010). A compressor map is usually measured as follows. Turbine inlet pressure and temperature are controlled to maintain a desired $\overline{N}$. A valve on the compressor discharge side is used to vary the back pressure of the compressor, and thereby $\overline{W}$ and Π_c. The system is given an appropriate time to stabilize all components thermally at a fixed discharge valve position, before a stationary compressor map point is measured. Points are then measured from surge up to choke. Different standards on how to measure and present map data exist, see e.g. SAE standard (1995a, 1995b), ASME (1997), and Chapman and Shultz (2003).

The definition of surge from SAE standard (1995b) has been analyzed in Galindo et al. (2006) and Andersen, Lindström, and Westin (2009), and different measures can be used e.g. pressure or shaft speed oscillations, or increasing temperature of air close to the impeller entry. A unique broadly accepted definition seems to be lacking. Surge is, in fact, a system property (Greitzer, 1981), and compressor characteristics can well be measured down to zero flow (Fink, Cumpsty, & Greitzer, 1992), and also reversed flow (Galindo, Serrano, Climent, & Tiseira, 2008). Down to what Π_c a speed line should be measured for larger flows is also an open question.

3. Experimental data

This section describes the stationary map database, and the dynamic measurements that are used to generate knowledge and form the rationale for the control oriented model. A first analysis,

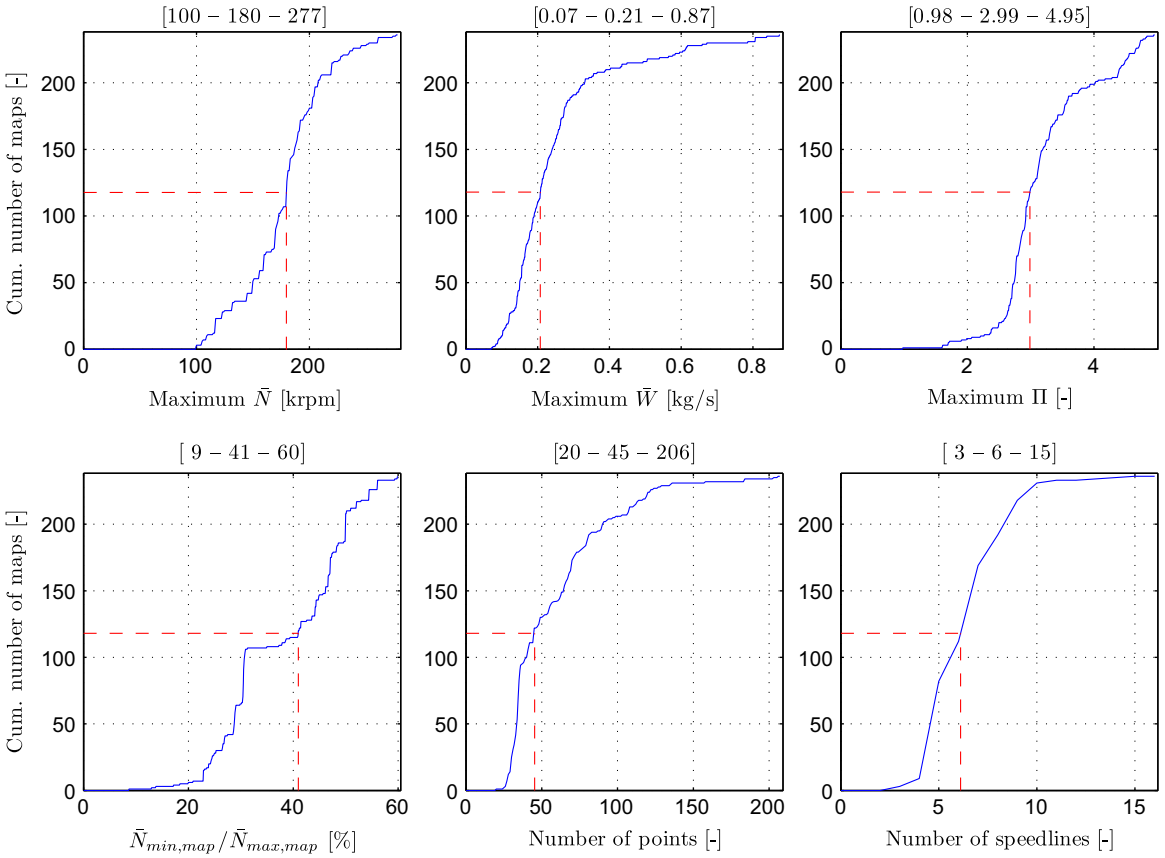

Fig. 2. Cumulative distribution of: maximum shaft speed, maximum corrected mass flow, maximum pressure ratio, ratio between minimum and maximum corrected shaft speeds, number of map points, number of speed lines, for the compressor map database. The title of each plots gives the minimum, and maximum value, and the cumulative sum equal to 50% of the number of maps in the database, respectively.

that serves as a preparation for the parametrization, is performed using the database.

3.1. Compressor map database

A database of compressor maps, with maps from the main manufacturers of turbos for automotive application, has been prepared. Fig. 2 summarizes the database, and presents cumulative distribution of: maximum shaft speed, maximum corrected mass flow, maximum pressure ratio, ratio between minimum and maximum corrected shaft speed, number of map points, number of speed lines, for the compressor map database. It can be seen that half of the maps have: (i) a minimum speed that is 41% or more of the maximum, (ii) 45 or more points, (iii) 6 or more speed lines. This is the type of data that one can expect when parametrizing a compressor model. A control oriented model structure should be capable of describing relevant performance from the average size map, given by roughly: 6 speed lines with roughly 7 points on each, where the lowest mapped speed line is 41% of the maximum found in the map. The typical map, of the 236 maps used to support the analysis of this paper, has: (1) a maximum $\overline{N}$ of 180 krpm, (2) a maximum $\overline{W}$ of 0.21 kg/s, and (3) a maximum Π_c of 2.99. The map database is thus biased towards car sized compressor maps. Some of the maps contain points measured down to a pre-defined minimum η_c. More rare are maps measured the whole way down to the discharge line characteristics of the gas stand. This line corresponds to the flow restriction the gas stand piping itself has, and is a function of the gas stand construction.

The slope $d\Pi_c/d\overline{W}$ of a SpL will be important in the latter analysis. Especially the slopes at the end points of a SpL are interesting, since these contain information of how a SpL can be extrapolated. For example, if a large negative slope exists at the maximum $\overline{W}$ of a SpL, the extrapolation of this SpL down to $\Pi_c = 0$ (below which compressor operation is physically impossible, since pressures cannot be negative) will be of good accuracy.

Fig. 3 shows the estimated speed line slope ($d\Pi_c/d\overline{W}$) for the points with smallest $\overline{W}$ of a SpL (left) and with largest $\overline{W}$ (right), for all maps in the database. The slopes were estimated as the slope of a straight line passing through the outer most two $\overline{W}$ points of each SpL. The x-axis is $\overline{N}$ normalized by the maximum $\overline{N}$ found in each map. A line is fitted to the data to illustrate the general trends. If these trend-lines are studied, it can be seen that the upper 40–50% of the $\overline{N}$ have a zero slope point between maximum and minimum flows, and thus that a zero slope point exists on that SpL-measurement. Further only the upper 40% of the speed lines have a significant negative slope at the maximum flow point, and thus enable an extrapolation of that SpL down to $\Pi_c = 0$. These observations will be important when selecting initial values for the optimization of the Ellipse flow model parameters, detailed in Section 5. There, e.g. the initial model parameters for $\overline{W}$ at the zero slope point of a SpL will be estimated from only the upper 40% of the map (since the lower part does not have a zero slope point).

3.2. Test stand experimental data

Test stand experimental data is collected from three different platforms: (i) a two stage turbocharged engine test stand (see Fig. 4(a)); (ii) a single stage engine test stand (see Fig. 4(b)); (iii) a compressor driven by a separate electric motor in a surge test

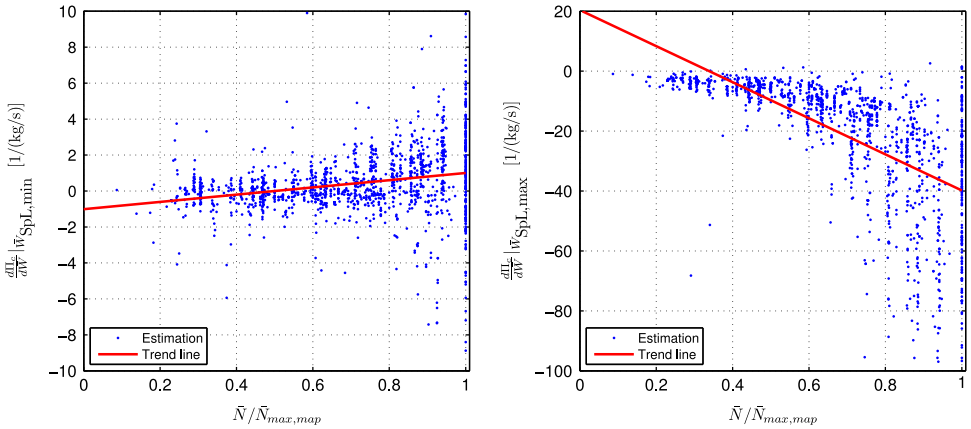

Fig. 3. Estimated speed line slope ($d\Pi_c/d\overline{W}$) for the points with smallest $\overline{W}$ of a SpL (left) and with largest $\overline{W}$ (right), for all maps in the database. The x-axis is $\overline{N}$ normalized by the maximum $\overline{N}$ found in each map. A line is fitted to the data, to illustrate the general trends.

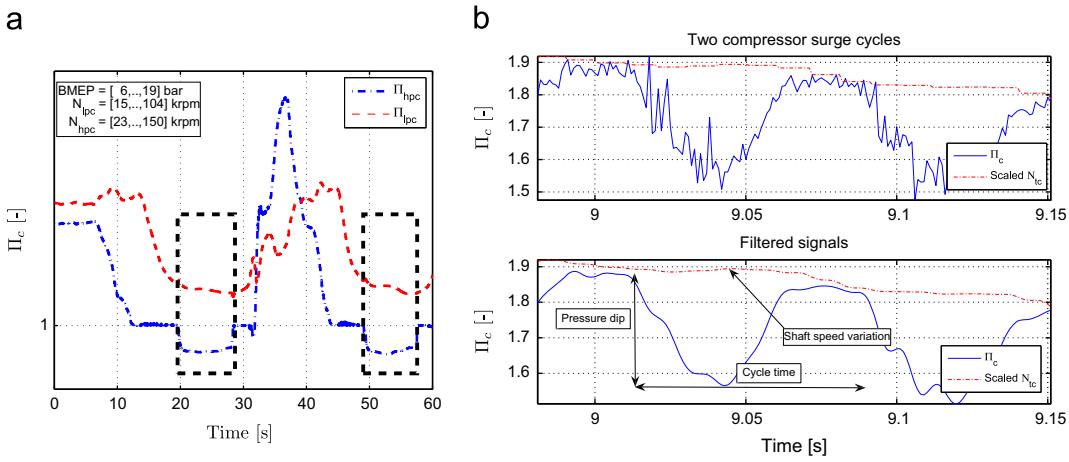

Fig. 4. Left: two stage system operating with the high pressure stage compressor as a restriction (with $\Pi_{c,HP} < 1$). Right: two measured surge cycles from a single stage test stand installation, indicating the surge properties discussed in Section 5.1. The solid line is zero phase shift low pass filtered Π_c to easily separate the measurement signal (dash-dotted) from the noise. The dashed line shows turbo shaft speed. The dashed box shows one surge cycle. The surge properties are: $t_{sc} = 71$ ms and $\Gamma_{\Pi_{cs}} = (1.85-1.59)/(1.85-1) = 31\%$.

stand (see Fig. 5). Details of the measurement chain of the engine test stands can be found in Leufvén (2010).

The surge test stand consists of a turbocharger where the turbine side has been removed. The driving torque is instead supplied from an electric motor via a gearbox, see Fig. 5(a). The compressor side piping consists of a straight inlet pipe with measurement stations for pressure and temperature. The discharge pipe contains a throttle used to control the operating point and measurement stations for temperature, pressure and mass flow. N_{tc} is measured and controlled using the electric motor. Continuous surge operation was possible for long periods of time, see Fig. 5(b). The reader is referred to Andersen et al. (2009) for more details on the surge test rig setup and the measurement chain.

4. Control oriented compressor models and MVEM

This section reviews related flow models available in the literature, and introduces the mean value engine modeling (MVEM) used in Sections 5.5.1 and 6.

4.1. Modeling normal, choke and surge operation

The basic operation of automotive turbochargers is presented in e.g. Watson and Janota (1982) and Zinner (1985), and a vast range of compressor flow models for the *normal* operating region are available in the literature, see Moraal and Kolmanovsky (1999) for a control oriented summary. For control applications, the modeling approaches used range from pure curve fitting based models (e.g. Eriksson et al., 2002; Guzzella & Amstutz, 1998; Müller, Hendricks, & Sorenson, 1998), dimensionless number modeling (e.g. Jensen, Kristensen, Sorenson, Houbak, & Hendricks, 1991; Thomasson & Eriksson, 2011), and physics based models of different computational cost (e.g. Gravdahl & Egeland, 1997; Oh, Yoon, & Chung, 2002; Zhuge, Zhang, Zheng, Yang, & He, 2009).

Choking is discussed and modeled in Watson and Janota (1982). Dixon and Hall (2010) and Gravdahl and Egeland (1999) model the inducer, impeller and diffuser choke flow, assuming that all flow processes are adiabatic and that the fluid is a perfect gas. The choke mass flow, assuming that choking occurs in the impeller and that the flow is isentropic, is modeled in Gravdahl and Egeland (1997) and Swain (2005), and is still an active field, see e.g. Casey and Schlegel (2010). Restriction compressor operation is discussed in a number of papers, see e.g. Shaaban (2004), Müller et al. (2005), and Casey and Schlegel (2010), where the compressor is modeled as a typical turbine nozzle characteristic with poor efficiency.

Surge modeling is described in numerous papers. Compressor characteristic during surge is modeled e.g. in Hansen, Jørgensen, and Larsen (1981), Willems (1997), Rakopoulos, Michos, and

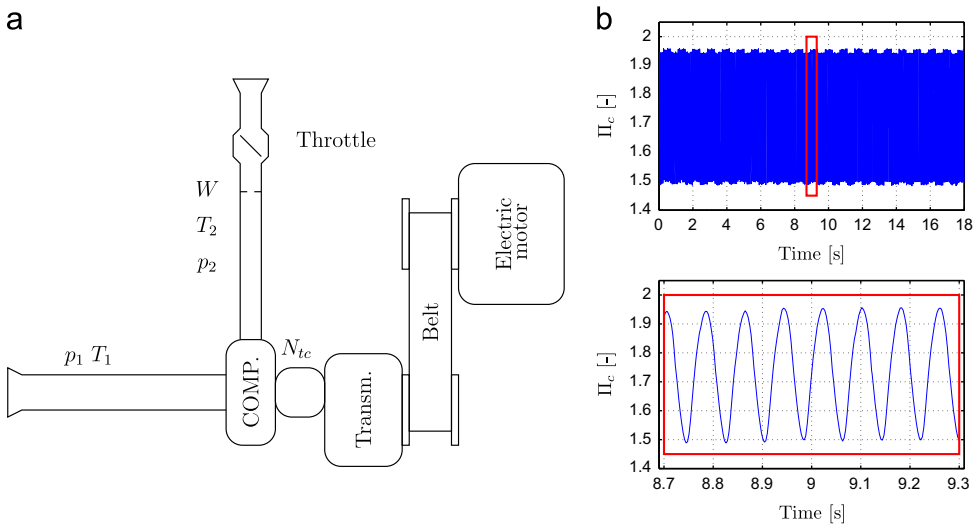

Fig. 5. Left: schematic overview of the surge test stand. Right: an example of continuous surge operation in the surge test stand. The lower plot shows the rectangle marked area of the upper plot enlarged.

Giakoumis (2005), Theotokatos and Kyrtatos (2001), and Grigoriadis (2008), where the most common model is a third order polynomial which is also used here. The process for reversed flow is modeled as isothermal (Galindo et al., 2008, 2011). Another important point of a full compressor characteristic is the zero flow pressure build up (denoted as $\hat{\Pi}_{c0}$ in the sequel), which is modeled e.g. in Theotokatos and Kyrtatos (2001), Grigoriadis (2008), Dehner, Selamet, Keller, and Becker (2010), Gravdahl, Willems, de Jager, and Egeland (2000), Gravdahl, Egeland, and Vatland (2001), Tauzia, Hetet, Chesse, Grosshans, and Mouillard (1998), Rakopoulos et al. (2005) using radial equilibrium theory. The radial equilibrium models have also been shown to give good fit to measured data in Galindo et al. (2008, 2011).

The model presented in this paper belongs to the grey-box family, where the physics is used in the basis functions to ensure sound extrapolation. Compared to previous efforts, all modes of operation are incorporated into the model structure, and no detailed geometric information is needed. The empirical basis functions improve the model fit, compared to pure physics based models, while still enabling automated parametrization and low computational cost.

4.2. Mean value engine modeling (MVEM)

The full system validation in this paper relies on MVEM, originally coined in Hendricks (1989) and Hendricks and Sorenson (1990). Component based MVEM of TC spark ignited (SI) engines is outlined in Eriksson et al. (2002) and Eriksson (2007). The baseline model is developed and validated in Andersson (2005) and has been extended to handle surge in Bergström and Leufvén (2007) and Leufvén and Eriksson (2008). The extension utilizes the model by Moore–Greitzer (Greitzer, 1981) that introduces a compressor mass flow state.

The TCSI model structure uses restrictions (air filter, compressor, intercooler, throttle, engine, turbine, exhaust system) interconnected with control volumes, and further extended with surge and wastegate valves. There are 14 states: six pairs of control volume pressures and temperatures, turbo shaft speed and compressor mass flow.

5. The compressor model

This section starts with a brief description of sub-models that commonly make up a compressor model, and the deep surge cycle properties that will be the goal of the surge modeling. The rest of the section is then devoted to the main contribution of the paper, the Ellipse compressor $\hat{\Pi}$–model.

To include surge capability in the compressor flow model, the approach in Greitzer (1981) is used, introducing a state for the compressor mass flow W_c according to

$$\frac{dW_c}{dt} = \frac{\pi D_c^2}{4L_c} \cdot (\hat{p} - p_c) \tag{3}$$

where

$$\hat{p} = \hat{\Pi} \cdot p_{af} \tag{4}$$

and D_c is the compressor diameter, L_c is the duct length. p_c and p_{af} are set by the system, while $\hat{p}$ (and $\hat{\Pi}$) is a measure of the pressure that the compressor builds given an operating point, and only for stationary operation is $p_c = \hat{p}$. This has implications for the highly non-stationary surge cycle. Here the rapid changes in $\overline{W}$ mean that there must be a large difference between the pressure measured in the control volume after the compressor (p_c) and $\hat{p}$ (the pressure in the control volume before the compressor times the modeled $\hat{\Pi}$), see the discussions in Section 5.5.

The compressor model has further sub-models describing: outlet temperature, T_c

$$T_c = T_{af}\left(\frac{\Pi_c^{(\gamma-1)/\gamma} - 1}{\eta_c} + 1\right) \tag{5}$$

and consumed torque, Tq_c

$$Tq_c = 30/\pi \frac{(T_c - T_{af}) c_p W_c}{N_{tc}} \tag{6}$$

where γ, c_p are gas properties taken as constants due to the small variations in inlet gas properties, and η_c is the compressor adiabatic efficiency. The η_c–model for all compressor operating regions from Leufvén and Eriksson (2011) is used here. The dynamics for the shaft speed N_{tc} are given by the turbo shaft torque balance

$$\frac{d(N_{tc}\pi/30)}{dt} = \frac{1}{J_{tc}}(Tq_t - Tq_c - Tq_{tc,fric}) \tag{7}$$

where Tq_t is the torque supplied from the turbine, $Tq_{tc,fric}$ is the shaft friction and J_{tc} is the turbocharger inertia.

5.1. Deep surge cycle properties

Two deep surge cycle properties, identified in Leufvén and Eriksson (2011), will be the goal of the surge modeling. A deep surge cycle is defined as a break down of flow through the compressor, followed by a rapid transition to fully reversed flow. The pressure after the compressor (p_c) then rapidly decreases, and the compressor is again able to maintain positive flow. A rapid transition to forward flow occurs, and p_c increases to end the cycle. The two deep surge cycle properties are

t_{sc}, cycle time of a deep surge cycle (s)

$$\Gamma_{\Pi_{cs}} = \frac{(\Pi_{c,max} - \Pi_{c,min})}{(\Pi_{c,max} - 1)} \ (-)$$

where $\Pi_{c,max}$ and $\Pi_{c,min}$ are the largest and smallest Π_c during a surge cycle. The properties are exemplified using engine test stand surge measurements in Fig. 4(b), which show also pressure and shaft speed variations for a typical surge cycle.

5.2. Ellipse compressor $\hat{\Pi}$−model

The model is divided into three distinct regions, depending on $\overline{W}$, to cover all operating modes. With reference to Fig. 1, these regions approximately correspond to: negative flow, unstable branch, and nominal and choke.

In this distinction, the point on a SpL with zero slope line (ZSL) is important. This point is not necessarily at the surge line, but is for most maps found close to the surge line (Hansen et al., 1981). Thus most map points have $\overline{W}$ larger than that at the ZSL. Two basis functions of the model structure describe the ZSL-points of a map; $\overline{W}$ at ZSL ($=\overline{W}_{ZSL}$), and $\hat{\Pi}$ at ZSL ($=\hat{\Pi}_{ZSL}$). It is then recognized that a compressor SpL falls of gradually with increasing $\overline{W}$. For large $\overline{W}$ the SpL tends to be vertical. This behavior is modeled as a generalized ellipse (motivating the model name) starting at the ZSL-point and having a vertical slope at a maximum $\overline{W}$ found at $\Pi_c = 0$. The maximum mass flow is described by a basis function in the model structure ($=\overline{W}_{max}$). The eccentricity of the ellipses (the SpL) is modeled using two basis functions ($=C_1$, C_2), and the model does have similarities, but does not strictly speaking correspond to an ellipse.

The model structure extends from the ZSL-point to a vertical slope at $\overline{W}_{max}$. The flow model, for normal operating, is thus made up by a generalized ellipse with its major and minor axes, as well as the eccentricity parametrized as a function of $\overline{N}$. The ellipse starts in the $(\overline{W}, \Pi_c)$-point $(\overline{W}_{ZSL}, \hat{\Pi}_{ZSL})$ and ends in $(\overline{W}_{max}, 0)$, with eccentricity given by C_1, C_2, see Fig. 1.

For positive $\overline{W}$ smaller than the ZSL, a third order polynomial is used as a model between the ZSL point and $\hat{\Pi}_{c0}$. The pressure build up at zero flow is in its turn modeled using $\Gamma_{\Pi_{cs}}$.

A turbine like behavior is used as a model for negative $\overline{W}$. This model is parametrized as three constants, independent of $\overline{N}$. The constants $\overline{W}_t$, $\hat{\Pi}_{ct}$ and K_{ct} give the shape of this turbine like characteristic.

To model equations are summarized as

$$\overline{W} > \overline{W}_{ZSL} \begin{cases} \hat{\Pi} = \left(1 - \left(\dfrac{\overline{W} - \overline{W}_{ZSL}}{\overline{W}_{max} - \overline{W}_{ZSL}}\right)^{C_1}\right)^{1/C_2} \hat{\Pi}_{ZSL} \\ C_1 = f_{C_1}(\overline{N}) \\ C_2 = f_{C_2}(\overline{N}) \\ \overline{W}_{max} = f_{\overline{W}_{max}}(\overline{N}) \\ \overline{W}_{ZSL} = f_{\overline{W}_{ZSL}}(\overline{N}) \\ \hat{\Pi}_{ZSL} = f_{\hat{\Pi}_{ZSL}}(\overline{N}) \end{cases}$$

$$0 < \overline{W} < \overline{W}_{ZSL} \begin{cases} \hat{\Pi} = \hat{\Pi}_{c0} + b_2\overline{W}^2 + b_3\overline{W}^3 \\ b_2 = 3(\hat{\Pi}_{ZSL} - \hat{\Pi}_{c0})/\overline{W}_{ZSL}^2 \\ b_3 = -2(\hat{\Pi}_{ZSL} - \hat{\Pi}_{c0})/\overline{W}_{ZSL}^3 \\ \hat{\Pi}_{c0} = \hat{\Pi}_{ZSL} - f_{\Gamma_{\Pi_{cs}}}(\overline{N})(\hat{\Pi}_{ZSL} - 1) \\ \Gamma_{\Pi_{cs}} = f_{\Gamma_{\Pi_{cs}}}(\overline{N}) \end{cases}$$

$$\overline{W} < 0 \left\{ \begin{aligned} \hat{\Pi} &= \hat{\Pi}_{c0} + (1 - (\overline{W}/b_1)^2)^{-1/K_{ct}} - 1 b_1 \\ &= \frac{\overline{W}_t}{\sqrt{1 - (\hat{\Pi}_{ct} - \hat{\Pi}_{c0} + 1)^{-K_{ct}}}} \end{aligned} \right. \quad (8)$$

where the parameters ($b_i, i \in 1,2,3$ and $\hat{\Pi}_{c0}$) are only intermediate variables, enabling the model SpL to be continuous in $\hat{\Pi}$ and the first derivative $d\hat{\Pi}/d\overline{W}$, at the two model region switching points ($\overline{W} = 0$ and $\overline{W} = \overline{W}_{ZSL}$).

The Ellipse flow model contains 14 parameters (denoted c) within the different basis functions to describe all the three quadrants of compressor operation. The following subsections will first describe the basis function f_i:

$$i \in \{C_1, C_2, \overline{W}_{max}, \overline{W}_{ZSL}, \hat{\Pi}_{ZSL}, \Gamma_{\Pi_{cs}}\} \quad (9)$$

and an automated model parametrization process will then be described. The normal operating region is first discussed, followed by surge modeling discussions.

It should be noted that the Ellipse model describes the connection between $\overline{W}$ and $\hat{\Pi}$. The motivation for this is that, while η_c presented in a map is largely affected by heat transfer, the flow/pressure-behavior is insensitive to changes in heat transfer, see e.g. Shaaban (2004), Cormerais, Hetet, Chesse, and Maiboom (2006), Casey and Fesich (2009), and Sirakov and Casey (2011). Thus, a detailed heat transfer modeling effort is avoided.

5.3. Normal region ($\overline{W} > \overline{W}_{ZSL}$)

Both $\overline{W}_{ZSL}$ and $\hat{\Pi}_{ZSL}$ are expected to increase with $\overline{N}$. For $\overline{N} = 0$, $\overline{W}_{ZSL} = 0$ and $\hat{\Pi}_{ZSL} = 1$ are expected. An increasing $\overline{W}_{max}$ with increasing $\overline{N}$ is expected, until the inducer chokes, see Gravdahl and Egeland (1997) and Dixon and Hall (2010).

5.3.1. Eccentricity: f_{C_1} and f_{C_2}

The first two Ellipse model functions enable an $\overline{N}$−dependent eccentricity of the ellipse (compare $((\overline{W} - \overline{W}_{ZSL})/(\overline{W}_{max} - \overline{W}_{ZSL}))^{C_1} + (\hat{\Pi}/\hat{\Pi}_{ZSL})^{C_2} = 1$). Five different versions of the eccentricity basis functions C_1 and C_2 were tested: a single constant $C_1 = C_2 = c_0$; a single affine function in $\overline{N}$ as $C_1 = C_2 = c_0 + c_1\overline{N}$; $C_1 = C_2 = c_0 + c_1\overline{N}^{c_2}$; $C_1 = C_2 = c_1 + c_2\overline{N} + c_2\overline{N}^2$; and finally the proposed structure as $C_1 = c_{1,0} + c_{1,1}\overline{N}$ and $C_2 = c_{2,0} + c_{2,1}\overline{N}^{c_{2,2}}$. The following f_{C_1} and f_{C_2} were found to balance model simplicity and descriptive capabilities for the map database

$$\begin{aligned} f_{C_1}(\overline{N}) &= c_{1,0} + c_{1,1}\overline{N} \\ f_{C_2}(\overline{N}) &= c_{2,0} + c_{2,1}\overline{N}^{c_{2,2}} \end{aligned} \quad (10)$$

where $c_{i,j}$ are real valued constants.

5.3.2. Maximum corrected mass flow: $f_{\overline{W}_{max}}$

A first order polynomial is proposed to model maximum corrected mass flow $\overline{W}_{max}$

$$f_{\overline{W}_{max}}(\overline{N}) = c_{3,0} + c_{3,1}\overline{N} \quad (11)$$

where $c_{3,0} > 0$ gives a positive flow also for $\overline{N} = 0$ (i.e. a standstill turbo), and $c_{3,1} > 0$ gives an increasing maximum $\overline{W}$ for increasing $\overline{N}$. A minimum selector can be added to physically correspond to a choked inducer flow, $\overline{W}_{ci}$, according to

$$\tilde{f}_{\overline{W}_{max}} = \min(\overline{W}_{ci}, f_{\overline{W}_{max}})$$

where the minimum selector emphasizes that no further increase in $\overline{W}$ is possible, independent of increases in $\overline{N}$. This was not used here.

If an ellipse SpL is fitted to each SpL of a map, the $\overline{W}_{max}$−values can be plotted against $\overline{N}$. Here it is important to note that in order for the Ellipse SpL to give reasonable extrapolation (down to $\Pi_c = 0$) focus should be on SpL with higher $\overline{N}$. This since these SpL will have the steeper slope at high $\overline{W}$. Fig. 6 presents normalized estimated maximum $\overline{W}$ (found at $\Pi = 0$) vs. normalized $\overline{N}$. Since the estimation relies on extrapolation using the slope of a SpL, only the upper SpL (with $\overline{N} > 60\% \cdot \max(\overline{N})$) are plotted. These SpL have a large slope, see Fig. 3. For smaller $\overline{N}$, with typically a small slope also at the maximum $\overline{W}$ of the SpL, the SpL-model parameter optimization typically resulted in a $\overline{W}_{max}$−estimate only slightly larger than the maximum $\overline{W}$ of that SpL, and with a very sharp eccentricity (C_1 and C_2).

An affine function is also fitted to the data and marked with a solid line (together with the best least squares fit parameters)

$$\frac{\overline{W}_{max}}{\overline{W}_{max,map}} = k_{3,0} + k_{3,1}\frac{\overline{N}}{\overline{N}_{max,map}} \tag{12}$$

Note that the indicated parameters $k_{3,0}$ and $k_{3,1}$ are deliberately indicated with k to separate them from the Ellipse basis function parameters c. The parameters k indicate the best fit between the C_3 normalized by the maximum flow of each map and $\overline{N}$ normalized by the maximum $\overline{N}$ of each map. The parameters are also fitted to all the maps of the database. However, the indicated parameters ($k_{3,0}$ and $k_{3,1}$) can be used as initial estimates for a model parameter optimization over all map points, given only $\overline{W}_{map,max}$ and $\overline{N}_{max,map}$.

5.3.3. Zero slope corrected mass flow: $f_{\overline{W}_{ZSL}}$

The equation for the zero slope mass flow model is

$$f_{\overline{W}_{ZSL}}(\overline{N}) = 0 + c_{4,1}\overline{N}^{c_{4,2}} \tag{13}$$

where the 0 emphasizes physically sound $\overline{W} = 0$ for $\overline{N} = 0$. An Ellipse SpL-model was parametrized to each map SpL (thus neglecting the $\overline{N}$−dependence in the model equations), using nonlinear least squares. Obtained $\overline{W}_{ZSL}$−points are presented in Fig. 7. Since the estimation tries to find the zero slope $\overline{W}$, only higher $\overline{N}$ (with $\overline{N} = 60\% \cdot \max(\overline{N})$) are plotted. This since lower SpL do not have a zero slope point, see Fig. 3.

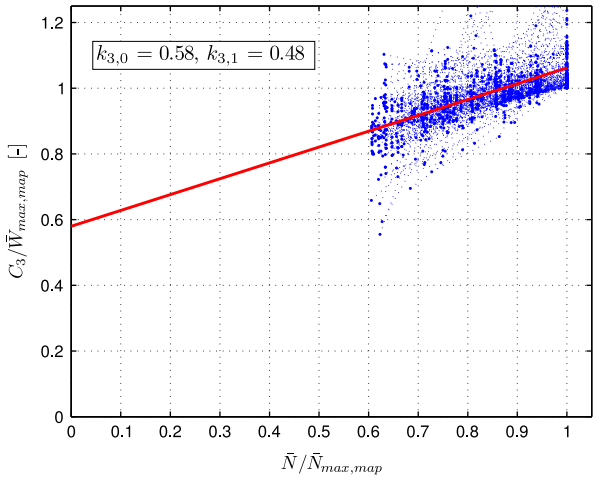

Fig. 6. Normalized estimated maximum $\overline{W}$ (found at $\Pi = 0$) vs. normalized $\overline{N}$. Since the estimation relies on extrapolation using the slope of a SpL, only the upper SpL (with $\overline{N} > 60\% \cdot \max(\overline{N})$) are plotted. These SpL have a large slope, see Fig. 3. A function of the form (11) is also fitted to all these normalized data points, and marked with a solid line (together with the function parameters).

The $\overline{W}_{ZSL}$ and $\overline{N}$ are here normalized by the maximum $\overline{W}$ and maximum $\overline{N}$ found in each map, respectively. In Fig. 7, each point represents a single speed line of a map. The points for each SpL of a map are connected with a dashed line. The proposed basis function (13) gives a good description. The red solid line is the least squares fit to all points of all maps of the database, and can be used as initial parameter estimates given only $\overline{W}_{map,max}$ and $\overline{N}_{max,map}$. It is important to note that the proposed Ellipse structure basis function $\overline{W}_{ZSL}$ is parametrized to a single map in applications, while the figure shows all maps together (thereby giving the "noisy" look). As in Section 5.3.2, the model parameters indicated in the figure can be used as initial values in an optimization using the maximum flow and speed found in a map (to go from k_{4j} to c_{4j}).

5.3.4. Zero slope pressure ratio: $f_{\hat{\Pi}_{ZSL}}$

The pressure ratio at the zero slope point is modeled as

$$f_{\hat{\Pi}_{ZSL}}(\overline{N}) = 1 + c_{5,1}\overline{N}^{c_{5,2}} \tag{14}$$

where the 1 emphasizes physically sound $\hat{\Pi} = 1$ for $\overline{N} = 0$. As in Section 5.3.3, Ellipse model parameters were estimated for each SpL of each map in the database. All $\overline{N}$ were used, since all SpL contain a maximum Π_c, either as a local maximum or in the point near the surge that is a point with a small slope.

The pressure ratio at the zero slope point is shown in Fig. 8. In the figure each point represents a single SpL of each map, and the points of each map are connected using dashed lines. The solid red line represents the least squares best fit for all maps of the database. Given the normalization as indicated by the axis, the line shows remarkable agreement for all points. As in the previous two sections, the indicated parameter values can be used as initial values for a model parameter optimization (using the maximum Π_c and $\overline{N}$ of a map to go from k_{5j} to c_{5j}). Two points can be made here. Since normal compressor operation is mainly in regions with a small SpL slope, the basis function (14) can in itself be used as a compressor flow model for this region, e.g. assuming the speed lines to be horizontal. Further, given only values of $\Pi_{c,max}$ and $\overline{N}_{max}$ the parameter values indicated in Fig. 8, together with the normalization, can be used if no map at all exists as

$$\hat{\Pi} = (\Pi_{c,max} - 1)\left(1 + k_{5,1}\left(\frac{\overline{N}}{\overline{N}_{max}}\right)^{k_{5,2}}\right) + 1$$

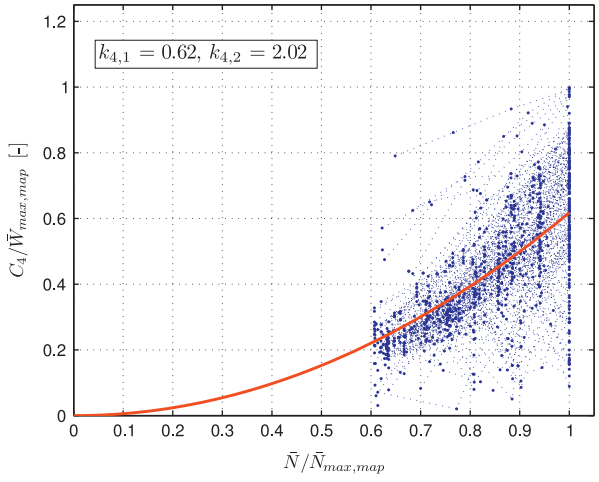

Fig. 7. Normalized $\overline{W}$ at the zero slope point of maps vs. normalized $\overline{N}$. Since the estimation tries to find the zero slope $\overline{W}$, only higher $\overline{N}$ (with $\overline{N} > 60\% \cdot \max(\overline{N})$) are plotted. This since lower SpL do not have a zero slope point, see Fig. 3. A basis function of the form (13) fitted to all the normalized data points is also shown. (For interpretation of the references to color in this figure caption, the reader is referred to the web version of this article.)

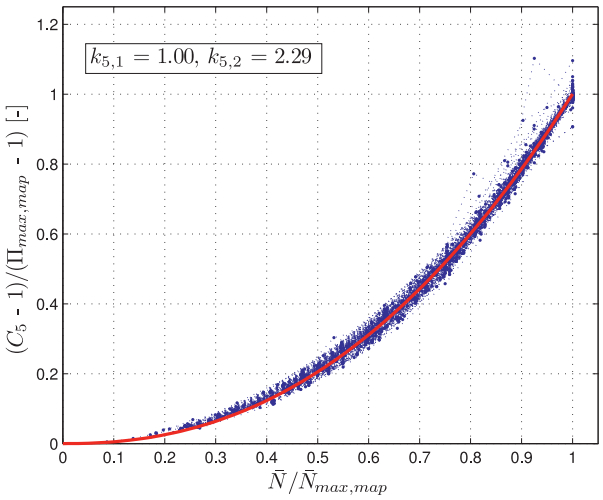

Fig. 8. $(\hat{\Pi}_{ZSL}-1)/(\hat{\Pi}_{max,map}-1)$ for each SpL of each map in the database vs. (map) normalized $\overline{N}$. Each point in the plot represents estimation on a single SpL of each map. (For interpretation of the references to color in this figure caption, the reader is referred to the web version of this article.)

For compressor models making use of interpolation, it is recommended to exploit the inherent curvature seen in Fig. 8, especially if the map grid is sparse in $\overline{N}$. This since using a linear interpolation can result in poor approximation.

5.3.5. Zero flow pressure ratio: $f_{\hat{\Pi}_{c0}}$

The experimental data indicates that $\Gamma_{\Pi_{cs}} \approx 30$–$35\%$ is a good approximation if no surge data exists. $\Gamma_{\Pi_{cs}} = 30\%$ is also chosen as the initial value for the parametrization process described in the next section. For compressor maps having points with lower mass flow than the zero slope line, another method can be used to shape the speed lines. Given the model structure from (8), nonlinear optimization can be used to find the parameters of $f_{\hat{\Pi}_{c0}}$ to obtain best fit to the map points. If no surge data is available for a map, the recommendation would be to use $\Gamma_{\Pi_{cs}} = 30\%$. This is indeed chosen for most of the maps of the database, due to the lack of surge data.

5.4. Parametrization for normal region

This section presents the automated parametrization process used to enable a quantitative analysis of the model structure. The process was necessary to avoid manually setting initial values for the full nonlinear least squares parameter optimization.

The process was divided into the following steps: (i) estimate the parameters of (9) for each $\overline{N}$; (ii) fit initial estimates of the C_{3-6} model parameters (denoted $\tilde{C}_{3-6}$); (iii) considering the initial estimates $\tilde{C}_{3-6}$ as locked, estimate initial C_{1-2}; and finally (iv) a full nonlinear least squares optimization starting at the initial values.

In the first step, a nonlinear least squares method was used. The initial conditions for the optimization were found from map values at the current SpL: $\tilde{C}_3 = 1.05 \cdot \max(\overline{W}_{SpL})$, $\tilde{C}_4 = \min(\overline{W}_{SpL})$, $\tilde{C}_5 = \max(\Pi_{c,SpL})$. The initial value for $\Gamma_{\Pi_{cs}}$ was set to 0.3, see Section 5.3.5. The initial values of the eccentricity parameters were put equal, and an iterative search with $\tilde{C}_1 = \tilde{C}_2 \in [1,9]$ was conducted. To avoid having less points than parameters to optimize over for a given SpL, eight points were added in close vicinity of the map points. The points were evenly distributed at a maximum distance of $\Delta\overline{W} = 0.5\% \cdot \max(\overline{W}_{SpL})$ from the map points. The pressure ratio of these additional points was calculated using estimates of the SpL slope for each map point.

The parameters $\tilde{C}$ estimated for each individual SpL were then used to make initial estimates of the corresponding basis function parameters $\tilde{c}_{ij}$, $i \in [1,6]$. The parameters $\tilde{C}_j$, $j \in \{1,2,3,4,6\}$, were considered to be uncertain for SpL having $\overline{N} < 60\% \cdot \overline{N}_{max}$. This uncertainty in the parameters stem from the small slope of these lower SpL, thus making the nonlinear least squares insensitive to parameter changes for these $\overline{N}$. However, the $\hat{\Pi}_{ZSL}$−estimation is considered to be of good quality, since all SpL (of most maps) have their maximum Π at a point with a small slope, and the estimation of the $\hat{\Pi}_{ZSL}$−model parameters $\tilde{c}_{5,i}, i = 1,2$ was conducted over all $\overline{N}$ of the maps.

The initial parametrization of the eccentricity basis functions was conducted using least squares.

The criterion in the optimization for the fourth, and last step, was to minimize the squared distance between Π_{map} and $\hat{\Pi}_{model}$ for all map points. Modeled $\hat{\Pi}$ for $\overline{W}$ larger than the modeled maximum flow C_3 is not defined in the structure, and was taken as 0.

The initially estimated $\tilde{C}_{3-5}$ are presented in Figs. 6, 7 and 8, respectively. These figures thus show a single point for each individual SpL in all maps of the database, and the points from each map estimation are connected using dashed lines.

5.5. Surge modeling parametrization

This section first discusses surge modeling properties in general, and then describes how experimental data can be used to further analyze the model properties.

First it is recognized that the exact SpL shape, for $\overline{W} \in [0, \overline{W}_{ZSL}]$, is not of great importance for the surge behavior, see Hansen et al. (1981). It can also be seen in (3), where the change in p_c is given by the emptying and filling dynamic of the downstream control volume, and $\hat{p}$ is given by the compressor model. The slope of a SpL is positive in this region, Greitzer (1981), Fink et al. (1992), and Galindo et al. (2008), and the difference $(\hat{p}-p_c)$ is therefore large, and the region is passed quickly. The, for surge, important parameter $\hat{\Pi}_{c0}$ (pressure ratio at zero flow) has been recognized in e.g. Theotokatos and Kyrtatos (2001), and is here modeled as a function of the parameter $\Gamma_{\Pi_{cs}}$, see (8).

The importance of $\hat{\Pi}_{c0}$ comes from the fact that the Π_c−trajectory, during deep surge, has to enclose the point $(\overline{W} = 0, \hat{\Pi}_{c0})$. This is seen in (3), where $\hat{p}$ has to lead p_c to increase W_c and take the compressor out of reversed flow. The trajectory is given by the compressor characteristics and the system properties.

If surge simulations are studied in detail, it is revealed that $\Pi_c \approx \hat{\Pi}$ is a good approximation, apart from during the rapid transition periods when the compressor flow changes sign. Hence, maximum and minimum Π_c during a surge cycle approximately give $\hat{\Pi}_{ZSL}$ and $\hat{\Pi}_{c0}$ of the model, respectively. Measurement data of Π_c during surge can therefore be used to assess $\Gamma_{\Pi_{cs}}$. Further, the pressure $\hat{p}_0 = p_{af} \cdot \hat{\Pi}_{c0}$ is the pressure of the downstream control volume needed for the compressor to go from negative to positive W_c, which will affect t_{sc}.

5.5.1. Effect from $\Gamma_{\Pi_{cs}}$, $\overline{W}_t$, $\hat{\Pi}_{ct}$, K_{ct} on the surge properties

The intermediate variable b_1 is given by algebraic constraints (8), forcing all SpL through $(\overline{W}_t, \hat{\Pi}_{ct})$. To investigate how the other Ellipse model parameters affect the surge properties from Section 5.1, an MVEM of the surge test rig is used. Each of the four model parameters $(\Gamma_{\Pi_{cs}}, \overline{W}_t, \hat{\Pi}_{ct}, K_{ct})$, describing the characteristics for $\overline{W}$ less than the ZSL-point, is varied $\pm\{10\%, 30\%\}$ from nominal values of $\Gamma_{\Pi_{cs}} = 49\%$, $\overline{W}_t = -0.059$, $\hat{\Pi}_{ct} = 10$ and $K_{ct} = 0.5$. Measurement of deep continuous surge is compared to a simulation with the nominal values in Fig. 12, showing good agreement.

The resulting sensitivity in the surge properties is summarized in Table 1. The most important parameters are found to be $\Gamma_{\Pi_{cs}}$ (giving $\hat{\Pi}_{c0}$) and $\overline{W}_t$.

Table 1
Sensitivity of the surge properties with respect to changes in the Ellipse model parameters. The parameters are varied $\pm\{10\%, 30\%\}$ from nominal, $t_{sc} = 81$ ms and $\Gamma_{\Pi_{cs}} = 54\%$.

Surge prop. change	$\Gamma_{\Pi_{cs}}$	$\overline{W}_t$	$\hat{\Pi}_{ct}$	K_{ct}	Param. change
Δt_{sc}	19% (−20%)	−4% (5%)	0% (−1%)	−1% (1%)	+30% (−30%)
	6% (−7%)	−1% (1%)	0% (−0%)	−0% (0%)	+10% (−10%)
$\Delta\Gamma_{\Pi_{cs}}$	26% (−27%)	1% (−1%)	−0% (0%)	0% (−0%)	+30% (−30%)
	9% (−9%)	0% (−0%)	−0% (0%)	0% (−0%)	+10% (−10%)

Table 2
Surge test stand measurements in normal and continuous surge operation. Upper part: deep surge at different $\overline{N}$. $\Gamma_{\Pi_{cs}} \approx 50\%$ independent of $\overline{N}$. Lower part: one $\overline{N}$ with different $mean(W_{th})$. The two last rows show that, for deep surge, an increase in $mean(W_{th})$ with 10% only decreases $\Gamma_{\Pi_{cs}}$ with $< 1\%$.

N_{tc} [krpm]	$mean(W_{th})$ [g/s]	$\Pi_{c,max}$ [-]	$\Pi_{c,min}$ [−]	$\Gamma_{\Pi_{cs}}$ [−] (%)
80	15.0	1.35	1.17	51
91	17.8	1.45	1.23	49
99	21.9	1.53	1.26	51
110	25.0	1.66	1.33	50
120	28.5	1.79	1.39	50
131	30.4	1.96	1.48	50
140	38.5	2.10	1.54	51
130	55.1	1.88	1.87	2
130	49.0	1.89	1.88	2
130	42.9	1.90	1.87	3
131	42.6	1.91	1.87	4
131	37.9	1.94	1.82	13
131	33.0	1.94	1.48	49
131	30.4	1.96	1.48	50

5.5.2. Surge rig data

The test rig is further described in Andersen et al. (2009), and some of the data are presented in Table 2. $\Gamma_{\Pi_{cs}}$ is calculated using continuous surge measurements at constant $\overline{N}$, see Fig. 12, where the compressor is operated at a typical "limit cycle". $\Gamma_{\Pi_{cs}}$ is found to be $\approx 50\%$ for a wide range of $\overline{N}$ for this compressor. Further, if several data sets with $\overline{N} = const$ are studied in more detail, it is found that once deep surge is established, $\Gamma_{\Pi_{cs}}$ shows only a small dependence of mean mass flow. Note that the third last row of Table 2 shows $\Gamma_{\Pi_{cs}}$ for mild surge, and also that points with larger flow have a non-zero $\Gamma_{\Pi_{cs}}$.

5.5.3. Engine test stand data

Fig. 9 presents multiple typical surge measurements, seen as oscillations in e.g. pressures and turbo speed, at tip-out from an engine test stand. A number of tip-outs were initiated for each initial engine operating point, and a number of initial engine operating points were tested.

It can be seen that when deep surge is established, surge is repeatable with remarkable accuracy, although the behavior of the first and last cycles of the surge periods can differ, where some cycles show a mild surge behavior. The right plots show $\Gamma_{\Pi_{cs}}$, where an increasing trend in $\Gamma_{\Pi_{cs}}$ for decreasing Π_c can be seen. When the surge period is over $\Gamma_{\Pi_{cs}}$ goes to zero. Since N_{tc} decreases during the tip-outs, it is not possible to get a correct value of $\Gamma_{\Pi_{cs}}$. The maximum pressure ratio during a surge cycle ($\Pi_{c,max}$ of Section 5.1) is here taken as the peak following an associated $\Pi_{c,min}$−value, giving an approximation of $\Gamma_{\Pi_{cs}}$. An increasing trend in $\Gamma_{\Pi_{cs}}$ can be seen for decreasing Π_c.

6. Validation

The validation is divided into three parts. Normal operation modeling is first validated. The low speed extrapolation capability is then validated, followed by a surge modeling validation. Note

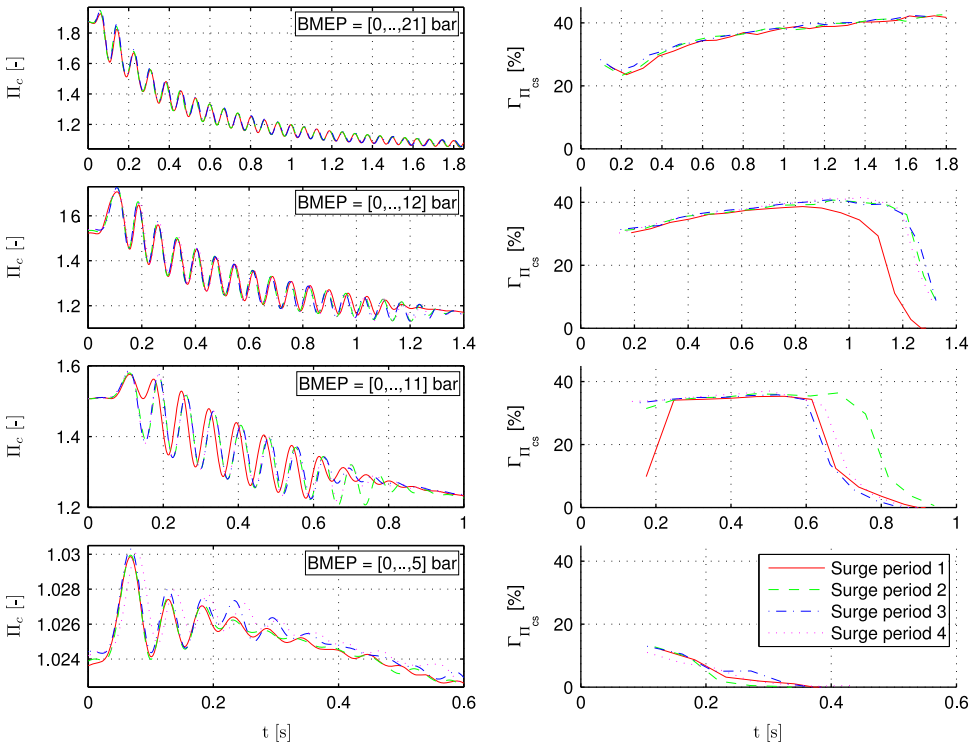

Fig. 9. Measured surge in an engine test stand. Each row shows multiple surge periods initiated from the same engine operating point. Initial Π_c decreases from top to bottom. Left: Π_c−traces. Right: calculated $\Gamma_{\Pi_{cs}}$.

that the models are parametrized on the component level, and that small component model errors might result in large errors on a system level. This can be handled following the methodology presented in e.g. Wahlström and Eriksson (2011), for which the model structure is well suited.

6.1. Normal operation

Normal operation was considered to be represented by the operating points in the compressor maps of the database. One should though keep in mind that some of the maps contained SpL measured down to very low η_c. Since the parametrization process of the model structure was automated, all maps in the database were used. A summary of the mean and maximum relative model errors is first presented. Three representative maps are then selected, and presented to show the model structure properties.

The model is compared to the map in Fig. 10. The left plot shows mean absolute relative error for map points with $\eta_c > 60\%$ ("normal" operating region), and for all map points. The right plot shows maximum absolute relative error. Note the different y-axis scalings of the plots. It can be seen that the mean errors are less than 2.5% and 4% for the $\eta_c > 60\%$ (normal operating range) and for all points respectively, for most of the maps. Also the maximum relative error for the normal operating range is small. It can also be seen that the Ellipse structure struggles for a few of the maps in the database. This can be a consequence of the least squares estimation getting stuck in a local minimum or a "strangely" shaped map.

Further validations are presented in Fig. 11. The figure presents what was considered to be three representative model fits (not the best, and not the worst fit models). Three compressors of different sizes were selected, representing flow ranges from (from left to right) a small car compressor up to a truck compressor. The circles represent map points, and the solid line is the Ellipse model. The model SpL are also extended down to maximum flow, and also down to zero flow to show the extrapolation. Very good agreement is found throughout the entire map for the small and large compressors, while the center model seems to underestimate $\overline{W}$ at ZSL of the map.

6.2. Surge operation

Mean value engine models (MVEM) are used to validate the surge modeling. Two models were constructed; one for the surge test stand, and one engine test stand.

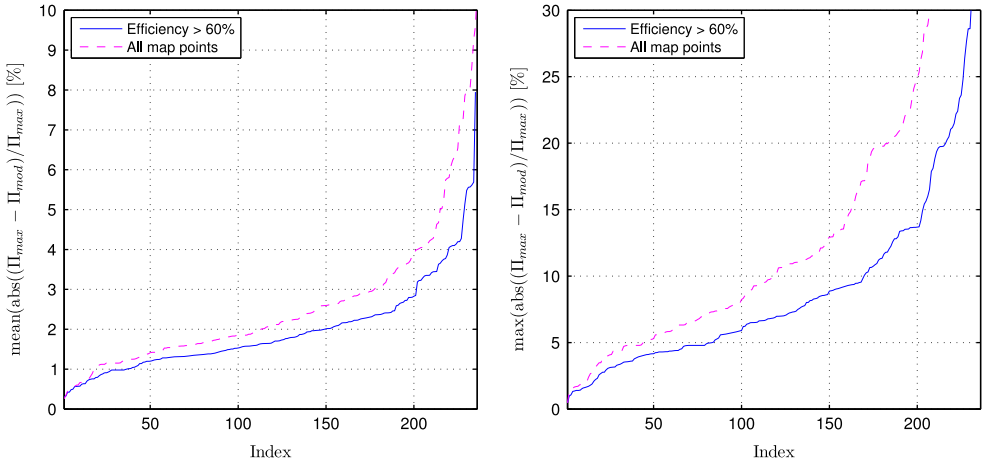

Fig. 10. Left: mean absolute relative error for map points with $\eta_c > 60\%$ ("normal" operating region), and for all map points. Right: maximum absolute relative error.

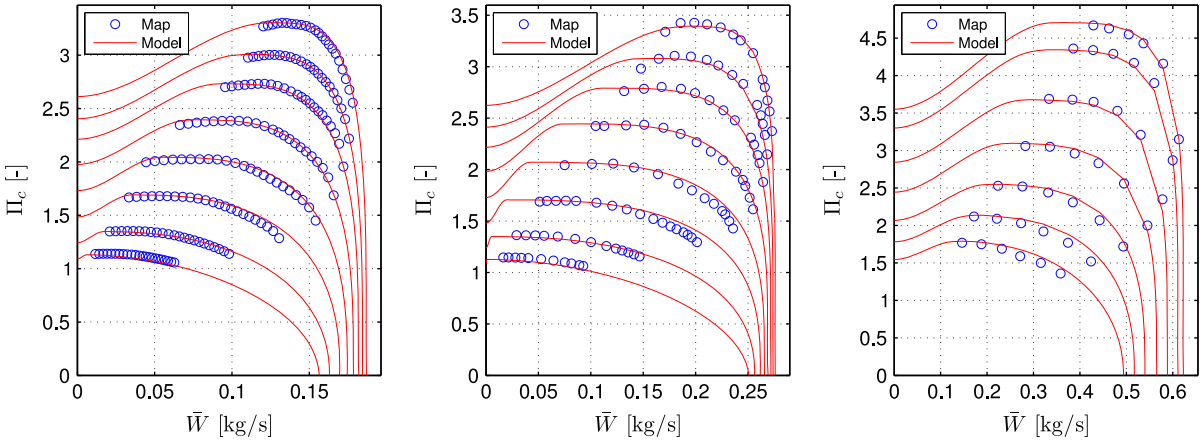

Fig. 11. Representative model fits for three different sized (from small car to truck application) compressors. The circles represent map points, and the solid line is the Ellipse model. Very good agreement is found throughout the entire map. The model SpL are also extended down to maximum flow, and also down to zero flow.

6.2.1. Surge test stand surge

The surge test stand MVEM consists of a compressor, two control volumes and a restriction. These are parametrized to correspond to the geometries and physical behavior from measurements. The results are shown in Fig. 12, where it is seen that measured and modeled t_{sc} and pressure oscillations are in good agreement. The upper plot shows a stable operating close to surge, where a good agreement between stationary modeled and measured Π_c is demonstrated. The lower plot shows an operating point in deep surge, where both the modeled t_{sc} and $\Gamma_{\Pi_{cs}}$ are in good agreement.

6.2.2. Engine test stand surge

The full TCSI MVEM developed in Andersson (2005) is extended with the Ellipse compressor model. The same engine used to parametrize the MVEM was driven in surge and measured. These measurements are here compared to the extended MVEM. The measured and modeled pressure oscillations are well modeled both in amplitude and frequency, both for stable operation before surge is initiated and during deep surge, see Fig. 13. The last modeled surge cycle deviates slightly from the measured, indicating a small error in t_{sc}.

7. Low speed extrapolation capability

Many of the available compressor maps contain measured points starting at approximately half of $\overline{N}_{max}$, see Fig. 2. All compressors, though, are started from standstill at some occasion, and many automotive applications make use of only the lower part of the compressor map (unless operated at altitude, see e.g. Leufvén & Eriksson, 2012; Olsson, 2007). The extrapolation capability of the model structure is thus important, in particular since compressor speed lines found in a map commonly represent only the upper half of the compressor $\overline{N}$ range, see Fig. 2.

This investigation makes use of the compressor maps, where measurements for low speed lines are available. An Ellipse model is parametrized using only the upper half $\overline{N}$ of the map, and the extrapolation capability of the model is then validated against the measured lower SpL of the maps.

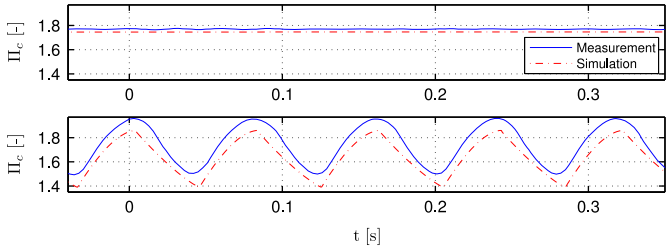

Fig. 12. Modeled and measured surge rig Π_c, for a constant $\overline{N} = 130$ krpm for two W_{th}. Upper: W_{th} close to surge. Lower: operating point with deep surge.

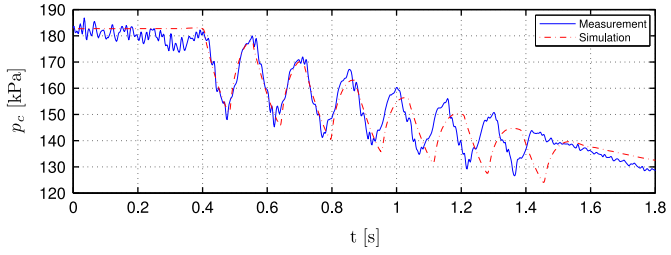

Fig. 13. Engine test stand measured and MVEM simulated compressor control volume pressure for a surge transient.

A total of 29 compressor maps were extracted out of the database. The selection criteria were that the maps should have: $\min(\overline{N}_{map}) < 0.3 \cdot \max(\overline{N}_{map})$, at least 90 points, and $\max(\Pi_{map}) > 2.8$. The maps passing these criteria were having $\overline{W}_{max,map} \in [0.1, 0.34]$ kg/s, and thus mainly of car or small truck sizes. The model parameter re-optimization to only the upper $\overline{N}$ was conducted using nonlinear least squares. The starting point for this optimization was the optimized parameters for all $\overline{N}$. During the re-optimization, the model parameters that changed the most were c_{41} and c_{51} (indicating a high model parameter sensitivity for these parameters).

The resulting mean and maximum absolute relative errors are presented in Fig. 14. It can be seen that the extrapolation capability of the Ellipse model structure is good, but for a few of the maps the extrapolation is less accurate. The lower SpL points (which was not included in the parametrization) have mean relative errors of less than 3% for most of the maps, for both map points with more than $\eta_c > 60\%$ and for all points. Also the maximum errors found are small.

8. Summary and conclusions

A database of 236 compressor maps has been analyzed, showing several interesting properties. A normal compressor map contains approximately 45 points over 6 speed lines, with shaft speeds starting at 41% of maximum shaft speed. A zero slope point and a significant negative slope at the maximum mass flow are normally only found for speed lines with $\overline{N} > 60\% \cdot \max(\overline{N})$. The knowledge generated from the database is used to build a compact but descriptive control oriented compressor model.

Normal and choke compressor operations can be modeled using ellipses, and extended to describe surge. The parametrization can be automated given a compressor map and data from surge. The proposed basis functions for the curve fitting are validated on a database of compressor maps, and are shown to give good description for a wide range of automotive compressors, both single stage and two stage. The basis functions are physically motivated, and ensure a sound extrapolation capability. The ellipse model has good performance for normal operation, as well as for surge and operation with pressure ratios less than unity.

The automated parametrization is shown to give less than 3% mean absolute relative error for the normal operating region, for more than 200 of the maps. The corresponding maximum absolute relative error is less than 15% for all normal points, for more than 200 of the maps. Good extrapolation capability is important since no data is available for lower turbo speeds. Linear interpolation between different speed lines is an approximation, and the interpolation is better handled using the proposed Ellipse structure. Especially the very good fit of the $\hat{\Pi}_{\mathrm{ZSL}}$–basis function can be exploited. The Ellipse model structure is shown to extrapolate to small turbo speeds with good performance.

The conclusions of the surge rig and engine test stand experiments are that $\Gamma_{\Pi_{cs}}$ can be used to model $\hat{\Pi}_{c0}$. If no available surge data exists, a constant value of $\Gamma_{\Pi_{cs}} \in [30, 50]\%$ will give a good approximation. Further, deep surge cycles are highly repeatable, and $\Gamma_{\Pi_{cs}}$ shows only a small dependency of mean mass flow. Surge pressure oscillations can be seen in measured data down to pressure ratios of close to unity, and are not limited to high pressure ratios/high shaft speeds. The deep surge cycle frequency is mainly given by the emptying and filling dynamics in combination with the compressor characteristics, where pressure build up at zero mass flow is most important. An MVEM together with the proposed Ellipse model can be used to model compressor surge with good accuracy.

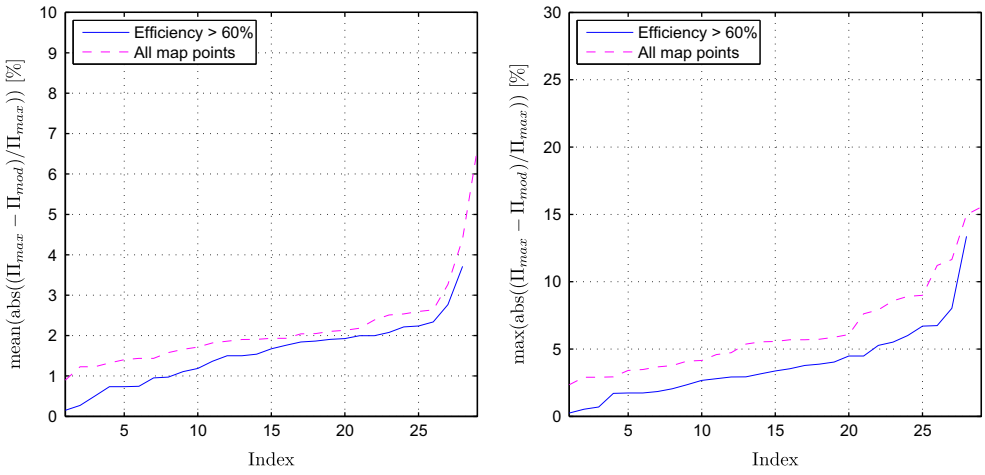

Fig. 14. Absolute relative errors for extrapolated low speed points. Left: mean values for map points with $\eta_c > 60\%$, and for all map low $\overline{N}$ points. Right: maximum absolute relative error. Note the different y-axis scalings of the plots. One of the maps did not have any point with $\eta_c > 60\%$ at the small $\overline{N}$ investigated.

Appendix A. Nomenclature

Symbol	Description
map	compressor map
01	compressor inlet station
02	compressor outlet station
af	air filter
c	compressor
*c*0	compressor at zero flow
cs	compressor surge
ct	compressor as turbine
fric	friction
hpc	high pressure stage
lpc	low pressure stage
max	maximum
min	minimum
$\Pi_{c,max/min}$	max/min Π_c during sc
sc	surge cycle
std	standard/reference
t	turbine
ci	choked inducer
tc	turbocharger
th	throttle
$\Gamma_{\Pi_{cs}}$	$(\Pi_{c,max}-\Pi_{c,min})/(\Pi_{c,max}-1)$ for sc
ZSL	zero slope line, $\overline{W} > 0$
SpL	speed line
p	pressure
Π	pressure ratio
Π_{c0}	pressure ratio at zero flow
$\hat{p}$	pressure build up
$\hat{\Pi}$	pressure build up ratio
$\hat{p}_0$–$\hat{p}$	at zero flow
$\hat{\Pi}_{c0}$–$\hat{\Pi}$	at zero flow
η	adiabatic efficiency
Γ–Π	ratio during surge
T	temperature
Tq	torque
W	mass flow
$\overline{W}$	corrected mass flow
N	shaft speed
$\overline{N}$	corrected shaft speed
D_c, L_c	characteristic diameter and length
γ, c_p	gas properties
J	inertia
t	time
$\overline{W}_t$	$\overline{W}$ at turbine-asymptote
$\hat{\Pi}_{ct}$	$\hat{\Pi}$ at turbine-asymptote
K_{ct}	turbine-asymptote parameter
C_1, C_2	Ellipse eccentricity
$\overline{W}_{max}$	maximum flow at $\Pi_c = 0$
$\overline{W}_{ZSL}$	$\overline{W}$ at ZSL
$\hat{\Pi}_{ZSL}$	$\hat{\Pi}$ at ZSL
$\Gamma_{\Pi_{cs}}$	modeled $\Gamma_{\Pi_{cs}}$
$c_{i,j}$	Ellipse model parameters
k_{ij}	model parameters fitted normalized data from all maps of the database

References

Andersen, J., Lindström, F., & Westin, F. (2009). Surge definitions for radial compressors in automotive turbochargers. *SAE International Journal of Engines, 1*, 218–231.

Andersson, P. (2005). *Air charge estimation in turbocharged spark ignition engines*. Ph.D. Thesis 989. Linköping University.

ASME. (1997). *PTC 10-1997, Performance test code on compressors and exhausters*. New York: American Society of Mechanical Engineers.

Bergström, J., & Leufvén, O. (2007). *Surge modeling and control of automotive turbochargers*. Master's Thesis LiTH-ISY-EX-3999. Linköping University.

Borila, Y. (1988). A sequential turbocharging method for highly-rated truck diesel engines. In *SAE*. Technical Paper 860074.

Casey, M., & Fesich, T. (2009). On the efficiency of compressors with adiabatic flows. In *Proceedings of ASME turbo expo*. GT2009-59015.

Casey, M., & Schlegel, M. (2010). Estimation of the performance of turbocharger compressors at extremely low pressure ratios. *Proceedings of the IMechE, Part A: Journal of Power and Energy, 224*.

Chapman, K. S., & Shultz, J. (2003). *Guidelines for: Testing large-bore engine turbochargers*. Technical Report. The National Gas Machinery Laboratory Kansas State University.

Chasse, A., Moulin, P., Albrecht, A., Fontvielle, L., Guinois, A., & Doléac, L. (2008). Double stage turbocharger control strategies development. In *SAE World congress*. Technical Paper 2008-01-0988.

Cormerais, M., Hetet, J., Chesse, P., & Maiboom, A. (2006). Heat transfer analysis in a turbocharger compressor: Modeling and experiments. In *SAE World congress*. Technical Paper 2006-01-0023, Detroit, USA.

Dehner, R., Selamet, A., Keller, P., & Becker, M. (2010). Simulation of mild surge in a turbocharger compression system. In *SAE World congress*. Technical Paper 2010-01-2142.

Dixon, S., & Hall, C. (2010). *Fluid mechanics and thermodynamics of turbomachinery* (6th ed.). Butterworth-Heinemann.

Emmenthal, K., Hagemann, G., & Hucho, W. (1979). Turbocharging small displacement spark ignition engines for improved fuel economy. In *SAE*. Technical Paper 790311.

Eriksson, L. (2007). Modeling and control of turbocharged SI and DI engines. *Oil & Gas Science and Technology - Revue de l'IFP*, *62*, 523–538.

Eriksson, L., Lindell, T., Leufvén, O., & Thomasson, A. (2012). Scalable component-based modeling for optimizing engines with supercharging, E-boost and turbocompound concepts. *SAE International Journal of Engines*, *5*, 579–595.

Eriksson, L., Nielsen, L., Brugård, J., Bergström, J., Pettersson, F., & Andersson, P. (2002). Modeling of a turbocharged SI engine. *Annual Reviews in Control*, *26*, 129–137.

Fink, D., Cumpsty, N., & Greitzer, E. (1992). Surge dynamics in a free-spool centrifugal compressor system. *Journal of Turbomachinery*, *114*, 321–332.

Galindo, J., Arnau, F., Tiseira, A., Lang, R., Lahjaily, H., & Gimenes, T. (2011). Measurement and modeling of compressor surge on engine test bench for different intake line configurations. In *SAE World congress*. Technical Paper 2011-01-0370.

Galindo, J., Climent, H., Guardiola, C., & Domenech, J. (2009). Strategies for improving the mode transition in a sequential parallel turbocharged automotive diesel engine. *International Journal of Automotive Technology*, *10*, 141–149.

Galindo, J., Serrano, J., Climent, H., & Tiseira, A. (2008). Experiments and modelling of surge in small centrifugal compressor for automotive engines. *Journal of Experimental Thermal and Fluid Science*, *32*, 818–826.

Galindo, J., Serrano, J., Guardiola, C., & Cervelló, C. (2006). Surge limit definition in a specific test bench for the characterization of automotive turbochargers. *Journal of Experimental Thermal and Fluid Science*, *30*, 449–462.

García-Nieto, S., Martínez, M., Blasco, X., & Sanchis, J. (2008). Nonlinear predictive control based on local model networks for air management in diesel engines. *Control Engineering Practice*, *16*, 1399–1413.

Gravdahl, J., & Egeland, O. (1997). Speed and surge control for a low order centrifugal compressor model. In *IEEE international conference on control applications* (pp. 344–349).

Gravdahl, J., Egeland, O., & Vatland, S. (2001). Active surge control of centrifugal compressors using drive torque. In *Proceedings of IEEE conference on decision and control* (Vol. 2).

Gravdahl, J., Willems, F., de Jager, B., & Egeland, O. (2000). Modeling for surge control of centrifugal compressors: Comparison with experiment. In *Proceedings of IEEE conference on decision and control* (Vol. 2, pp. 1341–1346).

Gravdahl, J. T., & Egeland, O. (1999). Centrifugal compressor surge and speed control. *IEEE Transactions on Control Systems Technology*, *7*, 567–579.

Greitzer, E. M. (1981). The stability of pumping systems—The 1980 Freeman Scholar Lecture. *Journal of Fluids Engineering*, *103*, 193–242.

Grigoriadis, P. (2008). *Experimentelle Erfassung und Simulation instantionärer Verdichterphänomene bei Turboladern von Fahrzeugmotoren*. Ph.D. Thesis. Technischen Universität Berlin.

Guzzella, L., & Amstutz, A. (1998). Control of diesel engines. *IEEE Control Systems Magazine*, *18*, 53–71.

Guzzella, L., Wenger, U., & Martin, R. (2000). IC-engine downsizing and pressure-wave supercharging for fuel economy. In *SAE World congress*. Technical Paper 2000-01-1019.

Hansen, K. E., Jørgensen, P., & Larsen, P. S. (1981). Experimental and theoretical study of surge in a small centrifugal compressor. *Journal of Fluids Engineering*, *103*, 391–395.

Hendricks, E. (1989). The analysis of mean value engine models. In *SAE*. Technical Paper 890563.

Hendricks, E., & Sorenson, S. C. (1990). Mean value modelling of spark ignition engines. In *SAE international congress and exposition*. Technical Paper 900616.

Heywood, J. (1988). *Internal combustion engine fundamentals. McGraw-Hill series in mechanical engineering*. McGraw-Hill.

Höckerdal, E., Frisk, E., & Eriksson, L. (2011). EKF-based adaptation of look-up tables with an air mass-flow sensor application. *Control Engineering Practice*, *19*, 442–453.

Jensen, J., Kristensen, A., Sorenson, S., Houbak, N., & Hendricks, E. (1991). Mean value modeling of a small turbocharged diesel engine. In *SAE World congress*. Technical Paper 910070.

Kimmich, F., Schwarte, A., & Isermann, R. (2005). Fault detection for modern diesel engines using signal- and process model-based methods. *Control Engineering Practice*, *13*, 189–203.

Leufvén, O. (2010). *Compressor modeling for control of automotive two stage turbochargers*. Licenciate Thesis LiU-TEK-LIC-2010:32, Thesis No. 1463. Division of Vehicular Systems, Department of Electrical Engineering, Linköping University.

Leufvén, O., & Eriksson, L. (2008). Time to surge concept and surge control for acceleration performance. In *Proceedings of IFAC World congress* (pp. 2063–2068).

Leufvén, O., & Eriksson, L. (2010). Engine test bench turbo mapping. In *SAE World congress*. Technical Paper 2010-01-1232.

Leufvén, O., & Eriksson, L. (2011). Surge and choke capable compressor model. In *Proceedings of IFAC World congress* (pp. 10653–10658).

Leufvén, O., & Eriksson, L. (2012). Investigation of compressor correction quantities for automotive applications. *International Journal of Engine Research*, *13*, 588–606.

Moraal, P., & Kolmanovsky, I. (1999). Turbocharger modeling for automotive control applications. In *SAE World congress*. Technical Paper 1999-01-0908.

Moulin, P., & Chauvin, J. (2011). Modeling and control of the air system of a turbocharged gasoline engine. *Control Engineering Practice*, *19*, 287–297.

Müller, M., Hendricks, E., & Sorenson, S. (1998). Mean value modelling of turbocharged spark ignition engines. In *SAE World congress*. Technical Paper 980784, Detroit, USA.

Müller, M., Sumser, S., Fledersbacher, P., Rößler, K., Fieweger, K., & Bauer, H. (2005). Using the centrifugal compressor as a cold-air turbine. In *International conference on turbochargers and turbocharging*, London.

Nitta, J., Minato, A., & Shimazaki, N. (2011). Performance evaluation of three-stage turbocharging system for heavy-duty diesel engine. In *SAE World congress*. Technical Paper 2011-01-0374.

Nyberg, M., & Stutte, T. (2004). Model based diagnosis of the air path of an automotive diesel engine. *Control Engineering Practice*, *12*, 513–525.

Oh, H., Yoon, E., & Chung, M. (2002). Systematic two-zone modeling for performance prediction of centrifugal compressors. *Proceedings of the IMechE, Part D: Journal of Automobile Engineering*, *216*, 75–87.

Olsson, J. (2007). Boost limitation in a torque based engine management system. In *IFAC symposium advances in automotive control* (pp. 609–616).

Omran, R., Younes, R., & Champoussin, J.-C. (2009). Optimal control of a variable geometry turbocharged diesel engine using neural networks: *Applications on the ETC test cycle*. *IEEE Transactions on Control Systems Technology*, *17*, 380–393.

Petitjean, D., Bernardini, L., Middlemass, C., Shahed, S., & Hurley, R. (2004). Advanced gasoline engine turbocharging technology for fuel economy improvements. In *SAE World congress*. Technical Paper 2004-01-0988.

Rakopoulos, C., Michos, C., & Giakoumis, E. (2005). Study of the transient behavior of turbocharged diesel engines including compressor surging using a linearized quasi-steady analysis. In *SAE World congress. Modeling of SI and diesel engine 2005* (*SP-1969*). Technical Paper 2005-01-0225.

SAE standard (1995a). J1826 – Turbocharger gas stand test code.

SAE standard (1995b). J922 – Turbocharger nomenclature and terminology.

Shaaban, S. (2004). *Experimental investigation and extended simulation of turbocharger non-adiabatic performance*. Ph.D. Thesis. Leibniz Universität Hannover.

Shehata, R. S., Abdullah, H. A., & Areed, F. F. (2009). Variable structure surge control for constant speed centrifugal compressors. *Control Engineering Practice*, *17*, 815–833.

Sirakov, B., & Casey, M. (2011). Evaluation of heat transfer effects on turbocharger performance. In *Proceedings of ASME turbo expo*. GT2011-45887.

Swain, E. (2005). Improving a one-dimensional centrifugal compressor performance prediction method. *Proceedings of the IMechE, Part A: Journal of Power and Energy*, *219*.

Tauzia, X., Hetet, J., Chesse, P., Grosshans, G., & Mouillard, L. (1998). Computer aided study of the transient performances of a highly rated sequentially turbocharged marine diesel engine. *Proceedings of the IMechE, Part A: Journal of Power and Energy*, *212*, 185–196.

Theotokatos, G., & Kyrtatos, N. (2001). Diesel engine transient operation with turbocharger compressor surging. In *SAE World congress*. Technical Paper 2001-01-1241.

Thomasson, A., & Eriksson, L. (2011). Modeling and control of co-surge in bi-turbo engines. In *Proceedings of IFAC World congress* (pp. 13010–13015).

Wahlström, J., & Eriksson, L. (2011). Modelling diesel engines with a variable-geometry turbocharger and exhaust gas recirculation by optimization of model parameters for capturing non-linear system dynamics. *Proceedings of the IMechE, Part D: Journal of Automobile Engineering*, *225*, 960–986.

Watson, N., & Janota, M. (1982). *Turbocharging the internal combustion engine*. London: MacMillan.

Westin, F., & Burenius, R. (2010). Measurement of interstage losses of a twostage turbocharger system in a turbocharger test rig. In *SAE World congress*. Technical Paper 2010-01-1221.

Willems, F. (1997). *Modeling and control of compressor flow instabilities*. Report No. WFW 96.151. Faculty of Mechanical Engineering, Control Engineering Section Eindhoven University of Technology.

Zhang, Z., Deng, K., Wang, Z., & Zhu, X. (2008). Experimental study on the three-phase sequential turbocharging system with two unequal size turbochargers. In *SAE World congress*. Technical Paper 2008-01-1698.

Zhuge, W., Zhang, Y., Zheng, X., Yang, M., & He, Y. (2009). Development of an advanced turbocharger simulation method for cycle simulation of turbocharged internal combustion engines. *Proceedings of the IMechE, Part D: Journal of Automobile Engineering*, *223*, 661–672.

Zinner, K. (1985). *Aufladung von Verbrennungsmotoren. Grundlagen, Berechnungen, Ausführungen*. Springer Verlag.